Available online at www.sciencedirect.com
ScienceDirect
Proceedings of the Combustion Institute 33 (2011) 2523–2529
Proceedings of the Combustion Institute
www.elsevier.com/locate/proci

Inhibition of hydrogen–oxygen flames by iron pentacarbonyl at atmospheric pressure

I.E. Gerasimov [a,b], D.A. Knyazkov [b], A.G. Shmakov [b], A.A. Paletsky [b], V.M. Shvartsberg [b,*], T.A. Bolshova [b], O.P. Korobeinichev [a,b]

[a] Novosibirsk State University, Novosibirsk 630090, Russia
[b] Institute of Chemical Kinetics and Combustion, Novosibirsk 630090, Russia

Available online 6 August 2010

Abstract

The chemistry of inhibition of laminar premixed hydrogen–oxygen flames by iron pentacarbonyl at atmospheric pressure was studied experimentally and by numerical simulation. Flame speed and chemical structure were analyzed. Flame burning velocities and inhibition effectiveness were measured and simulated for various equivalence ratios. The concentration profiles of a number of Fe-containing products of $Fe(CO)_5$ combustion, including Fe, FeO_2, FeOH, and $Fe(OH)_2$, were first measured using probing molecular beam mass spectrometry in an atmospheric-pressure $H_2/O_2/N_2$ flame. A comparison of the experimental and modeling results shows that they are in satisfactory agreement with each other, indicating that the reaction mechanism proposed previously for flame inhibition by iron pentacarbonyl is adequate for predicting the chemical structure of flames. The key recombination stages of active species catalyzed by Fe-containing species for flames of various stoichiometries can be determined by calculations of the production rates of H and O atoms and OH radicals as well as by analysis of the kinetic model.

Keywords: Flame inhibition; Iron pentacarbonyl; Flame speed; Flame structure; Reaction mechanism

1. Introduction

The combustion chemistry of iron-containing compounds, including iron pentacarbonyl $Fe(CO)_5$, is of considerable interest from various points of view. First, $Fe(CO)_5$ is known to be an effective flame inhibitor [1–10]. Based on experimental results on inhibition of premixed and diffusion $CH_4/O_2/N_2$ flames, a kinetic mechanism for $Fe(CO)_5$ transformation in flames has been developed which includes catalytic recombination reactions of atoms and radicals [3,4]. Rumminger and Linteris [4] suggested that a decrease in flame speed with the addition of $Fe(CO)_5$ is due mainly to the recombination of H and OH, catalyzed by FeO and FeOH.

Spatial variations of temperature and atomic iron concentration in a low-pressure lean ($\phi = 0.37$) $H_2/O_2/Ar/Fe(CO)_5$ flame have been measured using laser-induced fluorescence [11,12]. It has been found that iron pentacarbonyl decomposes in the flame to produce atomic iron, which is then transformed to iron oxides and hydroxides. Based on the previously proposed mechanism [4],

* Corresponding author. Address: Institute of Chemical Kinetics and Combustion, Institutskaya St., 3, Novosibirsk 630090, Russia. Fax: +7 383 330 7350.
E-mail address: vshvarts@kinetics.nsc.ru (V.M. Shvartsberg).

1540-7489/$ - see front matter © 2010 The Combustion Institute. Published by Elsevier Inc. All rights reserved.
doi:10.1016/j.proci.2010.06.026

a reduced 12-step mechanism for flame inhibition by $Fe(CO)_5$ has been developed and validated by comparing measured and simulated concentration profiles of atomic iron.

A low-pressure, rich ($\phi = 2.3$, $\phi = [H_2]/[H_2]_{stoichiometric}$), laminar, premixed $C_3H_6/O_2/Ar$ flame doped with ferrocene has been studied experimentally using MBMS and LIF and by numerical simulations [13]. The flame temperature was obtained by two-line OH LIF measurements, and the additive was found to increase the post-flame temperature by 40 K. An MBMS analysis of the species profiles of important intermediates in flames with and without ferrocene doping revealed a slight increase in the maximum concentration of species such as CH_2O, C_5H_5, and C_6H_6. At the same time, the dopant slightly decreased the maximum concentration of the propargyl radical C_3H_3, which is known to be an intermediate in soot precursor formation. The measurements showed a decrease in flame velocity when ferrocene was added, which was not predicted by the model.

Staude and Atakan [14] carried out equilibrium calculations for iron-doped $H_2/O_2/Ar$ and $C_3H_6/O_2/Ar$ gas mixtures under combustion-relevant conditions. It is noteworthy that condensed Fe-containing compounds were considered in the calculations. The focus was placed on iron intermediates and the conditions under which condensed phases of iron or iron species could be expected in the flame. The stoichiometry ($\phi = 0.37$, 1, and 2.3), temperature (1000–2500 K), and pressure (0.03–1 bar) were varied, allowing a prediction of which gas-phase iron species might be expected in measurable concentrations under the flame conditions considered. The effect of the sampling probe on the composition of the combustion products, which are cooled during probing, was discussed.

The addition of $Fe(CO)_5$ or ferrocene $Fe(C_5H_5)_2$ to sooting flames under certain conditions reduces the soot concentration in the post-flame zone [15–18]. Two possible mechanisms have been proposed to explain the effect of iron-containing compounds on soot formation [11]. Understanding the mechanism by which Fe-containing compounds influence soot formation is of great fundamental and practical importance.

Considerable efforts have been made to develop methods for the synthesis of nanoparticles in flames [18–20]. This is a promising line of research since it offers a possibility of controlling chemical and phase compositions, crystalline structure, and size distribution of nanoparticles by varying the composition of the unburned gases and precursor loading. Various methods have been used to analyze the size distribution, morphology, and structure of Fe_2O_3 particles as a function of $Fe(CO)_5$ concentration in low-pressure $H_2/O_2/Ar$ flames [21,22].

The above-mentioned lines of research into the combustion chemistry of $Fe(CO)_5$ are interrelated because they all deal with chemical transformations of iron in flames. The reactions reducing soot formation can be expected to contribute to flame inhibition, but one of the main objectives of future research should be to investigate the combustion chemistry of iron. The most fruitful approach to studying combustion chemistry is to analyze the chemical structure of Fe-doped flames. However, experiments with the formation of Fe-containing particles in Fe-seeded flames present great difficulties, and flame structure measurements are few in number. Therefore, the mechanisms for flame inhibition have been validated only by comparing measured and calculated burning velocities of premixed flames and extinction strain rates of opposed-jet diffusion flames.

The goal of the present work was to validate the mechanism of flame inhibition by iron pentacarbonyl [4] by comparing measured and simulated speeds of atmospheric-pressure H_2/air flames for various equivalence ratios and by comparing measured and simulated spatial variations of concentrations of Fe-containing products of $Fe(CO)_5$ oxidation in $H_2/O_2/N_2$ flames at atmospheric pressure.

2. Experimental and modeling approaches

Inhibition effectiveness was studied using laminar, premixed, atmospheric-pressure H_2/air flames in the stoichiometry range of 0.6–5 with and without the addition of 100 ppm $Fe(CO)_5$.

The chemical structure was measured for a premixed, near-stoichiometric ($\phi = 1.1$) $H_2/O_2/N_2$ (0.236/0.107/0.657) flame stabilized on a flat burner at $P = 1$ bar and $T_0 = 30$ °C. The gas velocity near the burner surface was 107 cm/s or about 75% of the freely propagating flame speed. The choice of the unburned gas composition and dopant loading was determined by specific condition of flame probing (see below).

2.1. Flame speed measurements

Burning velocity was measured using a Mache–Hebra nozzle burner [23] and the total area method [24] by an image of the flame shadow. The burner consisted of a 60-cm long Pyrex tube with an area contraction ratio of 7.4 (over a 15 mm length) and a nozzle exit with an inner diameter of 5.5 mm. The nozzle contour was designed so as to obtain a straight-sided image of the flame-cone shadow. The estimated confidence interval for the burning velocity was about 5%.

The results were compared with experimental data obtained using alternative techniques [25]. In the range of equivalence ratio (0.6–1.2) of combustible mixtures, there is good agreement between literature and our data. Gas flows were

measured by mass-flow controllers (MKS Instruments Inc., model 1299S) calibrated with a wet gas meter with an accuracy of ±1%. The temperature of the combustible mixture was about 25 °C.

Shadow photography of the flame-cone was performed using an optical system consisting a light source, a lens, a diaphragm, and a semitransparent screen. The burner was placed between the diaphragm and the screen, and the flame shadow image was photographed on the back side of the screen.

2.2. Flame structure measurement using MBMS technique

The flat burner consisted of a porous (a pore size of about 0.05 mm) brass disc 16 mm in diameter and 3 mm thick, embedded in a brass housing equipped with a cooling jacket. The unburned gases were metered using mass-flow controllers (MKS Instruments Inc.). $Fe(CO)_5$ in an amount of 100 ± 10 ppm was added to the unburned gases by passing, together with carrier nitrogen, through an evaporator.

The flame structure was measured by molecular beam mass spectrometry (MBMS). To provide a working pressure of 10^{-3} Torr in the first stage of the MBMS sampling system, we used a 0.08-mm orifice probe (wall thickness 0.08 mm, inner angle 40°) for sampling from a flame at 1 bar. MBMS study of $Fe(CO)_5$-doped flames involves some procedural difficulties. First, the interaction of iron oxides with a quartz probe at high temperatures results in destruction of the probe. Second, relatively low flame temperatures lead to condensation of iron-containing species (ICS) and particle formation, which reduces the iron concentration in the gas-phase of the flame. In addition, the particles clog the orifice of the probe. Therefore, the composition of the combustible mixture was chosen so as to provide the maximum possible life of the probe and the maximum flame temperature (appropriate for using a quartz probe). The $Fe(CO)_5$ loading (100 ppm) was chosen so as to produce the minimum amount of particles in the flame that was sufficient for measuring ICS concentrations.

Spatial variation of ICS concentrations was measured using an MBMS setup equipped with a MS7302 quadrupole mass-spectrometer [26,27] with soft electron-impact ionization (spread of ionization energies ±0.12 eV). Soft ionization allows one to decrease or eliminate the contribution of fragmentary ions to the measured peak by setting the ionization energy close to the ionization potential of the compound.

Spatial variation in the intensities of the peaks at 56, 73, 88, and 90 AMU, which correspond to Fe, FeOH, FeO_2, and $Fe(OH)_2$, respectively, was measured at an ionization energy of 20 eV. The contribution of fragmentary ions to the peaks was determined by measuring the intensity ratios of the peaks at 56, 73, 88, and 90 AMU in a certain flame cross section at ionization energy of 12, 18, and 20 eV. It was found that the contribution of fragmentary ions did not exceed the error of the intensity measurement.

Since the ICS mole fraction was rather low (10^{-4} – 10^{-5}), the accuracy of their measurement was ±50%. The results were averaged over several sets of measurements. After each series of experiments (within 30 min), the probe was replaced by a new one.

An important aspect of the MBMS technique is the calibration of the setup against ICS. A direct calibration against ICS is impossible because of their low volatility. A comparison of modeling data and calculation results for the equilibrium concentration of ICS at the post-flame temperature revealed that, in the post-flame zone (2–3 mm above the burner), the ICS equilibrium concentrations were quite close to the simulated ones. This allowed us to determine the calibration coefficients by correlating the equilibrium concentrations with the peak intensities.

2.3. Modeling

Flame speed and the structure were calculated by using kinetic models for $H_2 + CO$ oxidation and a mechanism for flame inhibition by iron pentacarbonyl (60 reactions of 12 species: $Fe(CO)_5$–Fe(CO), Fe, FeO, FeOH, FeO_2, $Fe(OH)_2$, FeH, and FeOOH) [4]. The model for $H_2 + CO$ oxidation comprised 92 reactions of 26 species from GRI-Mech 3.0 [28].

To analyze the reaction pathways of Fe-containing species in the flame, we investigated Fe-element fluxes from species to species using the KINALC code [29], a post-processor of the output files of the PREMIX code [30,31]. Since the element flux analysis should be carried out with a reaction mechanism containing only irreversible reactions, the original mechanism [4,28] was first converted to irreversible form by using the MECHMOD code [32]. The Flux Viewer code [33] was used to visualize Fe-fluxes.

3. Results and discussion

3.1. Effect of iron on flame speed

Fig. 1 shows the flame speeds in H_2/air mixture without additives and those doped with 100 ppm atomic iron at a pressure of 1 bar versus equivalence ratio. Experimental data on the speed of the undoped flames [25] are also presented in Fig. 1. Good agreement between the reference experimental and modeling results confirms the validity of the chosen mechanism for the conditions considered. The modeling results show that

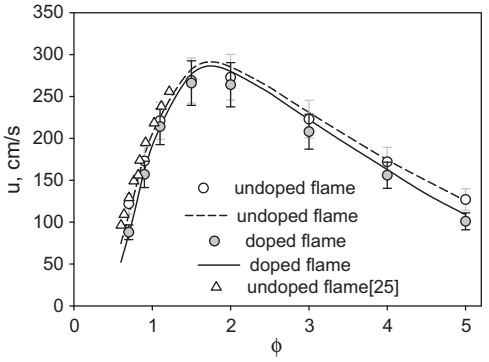

Fig. 1. Flame speed of atmospheric-pressure H_2/air mixtures without additive and doped with 100 ppm $Fe(CO)_5$ versus equivalence ratio; symbols – experiment, curves – modeling.

the inhibition intensity depends on ϕ of the unburned gases.

Fig. 2 shows the inhibition effectiveness expressed as the relative decrease in the flame speed due to the addition of the inhibitor ($F = (u_0 - u)/u_0$, where u_0 is the speed of the undoped flame and u is the speed of the Fe-doped flame) versus ϕ.

From the data in Fig. 2, it follows that the inhibition effectiveness is minimal at $\phi \approx 2$ for modeling data $\phi \approx 1.5$ for experimental results. It is noteworthy that in spite of a good agreement between measured and calculated flame speeds, the agreement between the experiment- and modeling-based inhibition effectiveness is rather poor. It is explained by a strong dependence of the confidence interval of the inhibition effectiveness on the error of the flame speed measurement (both undoped and $Fe(CO)_5$-doped one). A change in the unburned gases composition leads to an increase in the effectiveness, the inhibition being more effective in lean flames than in rich ones.

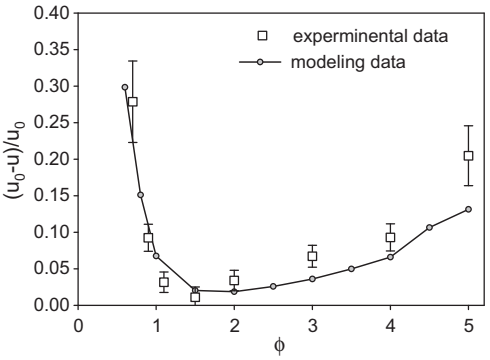

Fig. 2. Inhibition effectiveness of atmospheric-pressure H_2/air flames doped with 100 ppm $Fe(CO)_5$ expressed as the relative decrease in the flame speed due to inhibitor addition $(u_0 - u)/u_0$ versus equivalence ratio; symbols – experimental data, curve – modeling data.

3.2. Flame structure

Fig. 3 presents the simulated concentration profiles of $Fe(CO)_5$, Fe, FeO, FeOH, FeO_2, and $Fe(OH)_2$ in the flame doped with 100 ppm $Fe(CO)_5$. The FeH and FeOOH concentrations are too low and cannot be shown in the figure. One can see that $Fe(CO)_5$ is consumed in a narrow zone 0.2–0.3 mm, yielding other ICS. The ICS concentration varies over the flame zone but the main post-flame iron-containing component is iron hydroxide $Fe(OH)_2$. As is evident from Fig. 3, the main iron-containing species in the flame reaction zone is atomic iron.

The measured and simulated concentration profiles of Fe, FeOH, FeO_2, and $Fe(OH)_2$ in the $Fe(CO)_5$-doped flame are given in Fig. 4a–d, respectively. The intensity of peak at 72 AMU (FeO) was very low and we failed to measure it near the burner and along the flame zone. It may be explained by a low FeO concentration in the flame (contrary to the model prediction). Another reason may be connected with low sensitivity of mass-spectrometer to FeO. In our practice, we met examples when to parent compounds have essentially different calibration coefficients, e.g. $k_{PO2}/k_{PO} = 0.77/0.02 = 38.5$. By the same argument we failed to measure FeH and FeOOH. The Fe profile is obtained by taking into account the contribution of Fe^+ from iron pentacarbonyl molecules. According to the experimental data, the iron concentration profile has a maximum at 0.4 mm above the burner, whereas the modeling predicts that the iron profile is 0.6 mm above the burner (Fig. 4a). Thus, the results indicate that atomic iron is an intermediate product of $Fe(CO)_5$ destruction in flame, as has been shown previously using an alternative method of flame diagnostics [11].

A similar situation is observed for the FeOH concentration profile shown in Fig. 4b. The position of the maxima of the FeOH profile is pre-

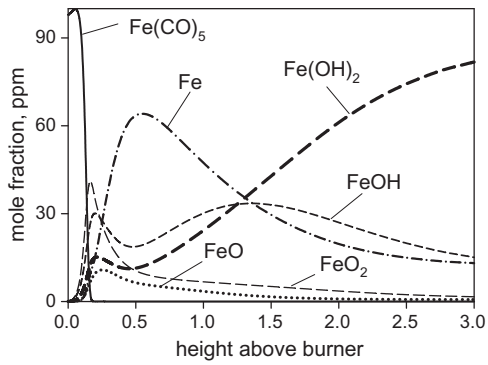

Fig. 3. Simulated spatial variations of ICS concentration in $H_2/O_2/N_2$ flame doped with 100 ppm $Fe(CO)_5$ stabilized on a flat burner at 1 bar.

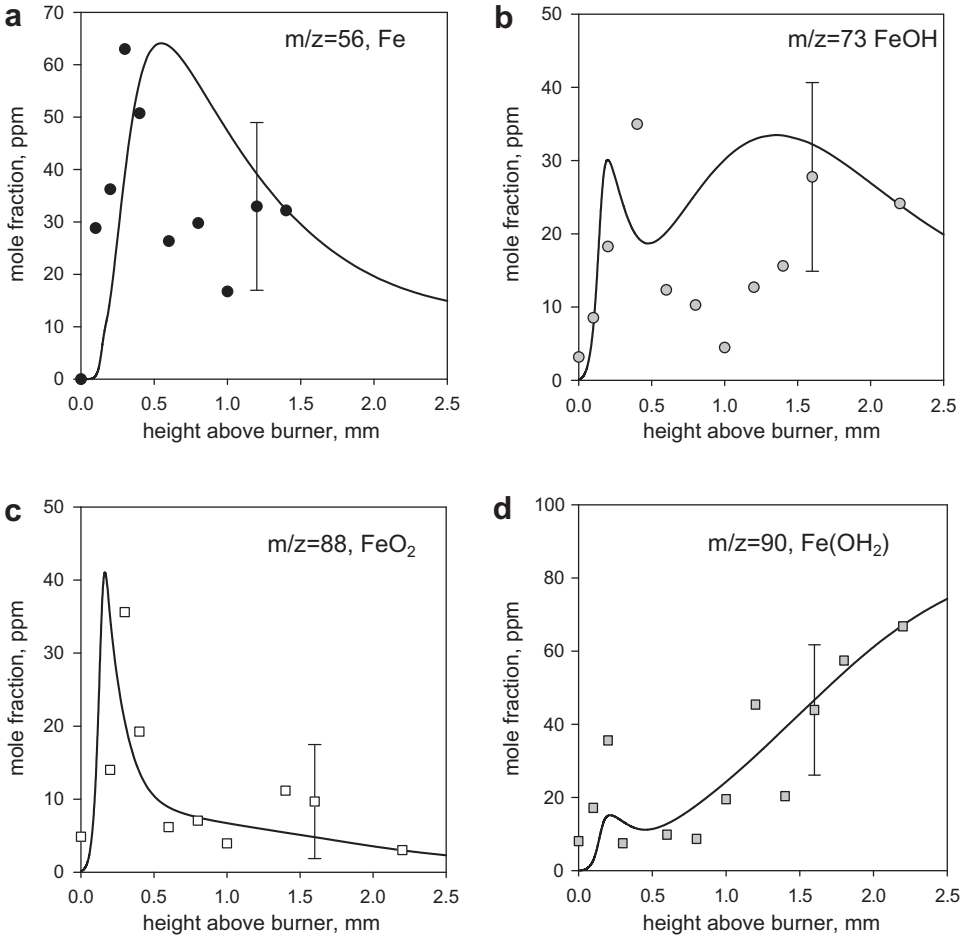

Fig. 4. Spatial variations of ISC concentration in $H_2/O_2/N_2$ flame doped with 100 ppm $Fe(CO)_5$ stabilized on a flat burner at 1 bar; symbols – experiment, curves – modeling.

dicted to be 0.2 and 1.5 mm above the burner, but the experimentally measured profile is slightly shifted relative the predicted one. Nevertheless, there is qualitative agreement between the modeling and experimental data.

It is evident from Fig. 4c that FeO_2 is an intermediate product of $Fe(CO)_5$ combustion. The maximum of its concentration profile is observed in the preheating flame zone at proximally 0.2 mm from the burner. Next, the FeO_2 concentration decreases monotonically.

Fig. 4d gives the measured and simulated concentration profiles of $Fe(OH)_2$. One can see that the experimental and modeling data are in satisfactory agreement. The measured and simulated profiles of the $Fe(OH)_2$ mole fraction have maxima at 0.2–0.3 mm above the burner. The $Fe(OH)_2$ concentration increases with distance from the burner, and reaches the level of 8×10^{-5}, which is 80% of all iron in the flame. Despite some discrepancies between the measured and predicted concentration profiles of $Fe(OH)_2$ in the preheating zone of the flame, the profiles are generally in satisfactory agreement. The same is true for the FeO_2 profile.

The experimental and modeled total concentration profiles of ICS versus height above the burner are given in Fig. 5. A comparison of these profiles shows that the experiment gives a 50% lower amount of iron at 0.5– mm from the burner than the predicted value. A possible explanation of this difference may be that the mass peak intensities of the ICS not involved in the mechanism [4] (for example, Fe_2O_3 and Fe_3O_4) were not recorded. If this explanation is true, the concentration profiles of the unrecorded compounds should have a maximum at 0.5–1 mm above the burner. The mass peaks of Fe_2O_3 and Fe_3O_4 are outside the mass range of the mass-spectrometer used (1–143 AMU) and, hence, were not recorded.

Analyzing the ability of the mechanism [4] to predict ICS concentrations, we can conclude that

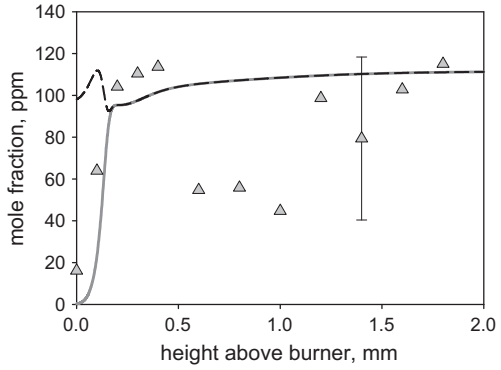

Fig. 5. Spatial variations of total ICS concentration in $H_2/O_2/N_2$ flame doped with 100 ppm $Fe(CO)_5$ stabilized on a flat burner at 1 bar; symbols – experiment, curves – modeling.

the model gives a satisfactory prediction of the ICS concentration in the height ranges of 0–0.5 and 1.2–2 mm. It can be suggested that the kinetic model for $Fe(CO)_5$ combustion can be refined by extending the number of the ICS considered and considering the flame reaction zone in greater detail.

An analysis of the $Fe(CO)_5$ transformation pathways in the flame revealed the key steps of its oxidation and ICS formation in the various flame zones. The reaction fluxes were calculated for cross sections of the flame at 0.12, 0.15, 0.3, and 1, 2 mm above the burner. Fig. 6 shows the ICS transformation fluxes at 0.3 mm above the burner. The transformation fluxes at 0.3 mm above the burner account for the situation in the flame reaction zone, i.e. the high rate of radical recombinations. In the reaction zone (0.2–0.6 mm above the burner), as O_2 is consumed, atomic iron is produced by the FeO reduction reaction involving H, O, and H_2:

$$FeO + O = Fe + O_2 \quad (1)$$

$$FeO + H = Fe + OH \quad (2)$$

$$FeO + H_2 = Fe + H_2O \quad (3)$$

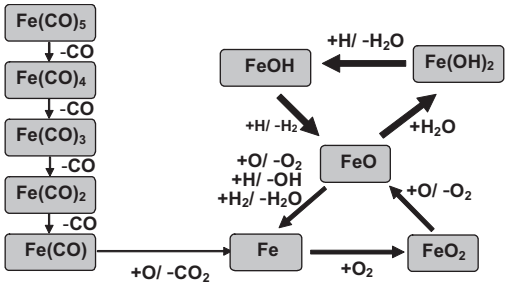

Fig. 6. Schematic diagram of ICS reaction pathways in $H_2/O_2/N_2$ flame doped with 100 ppm $Fe(CO)_5$. Thicker arrows correspond to higher reaction flux.

The rates of these processes are rather high due to the high concentrations of H and O atoms in this flame region. An analysis of the reaction fluxes revealed an insignificant contribution of OH to the ICS production and consumption rates, although the OH concentration is even higher than that of O atoms. The simulated profiles of H, O, and OH are shown in Fig. 7. The contributions of reactions (1)–(3) to the total rate of Fe production in this flame cross section are 35%, 35%, and 23%, respectively. In this cross section of the flame, following cycle can be noted:

$$FeO + H_2O = Fe(OH)_2 \quad (4)$$

$$Fe(OH)_2 + H = FeOH + H_2O \quad (5)$$

$$FeOH + H = FeO + H_2 \quad (6)$$

In the post-flame zone, Fe reacts with H and H_2O to produce FeOH and $Fe(OH)_2$ (reactions (3)–(6)). As can be seen from Fig. 6, FeO is a key ICS in the mechanism considered [4] because it provides interconversion of Fe, iron oxides, and hydroxides in a certain flame zone.

Rumminger and Linteris [5] showed that, in a $CO/H_2/O_2/N_2$ flame doped with iron pentacarbonyl there are two cycles of H and O recombination which include reactions 1, 7, 8 and reactions (4)–(6).

$$Fe + O_2 = FeO_2 \quad (7)$$

$$FeO_2 + O = FeO + O_2 \quad (8)$$

Our analysis of the reaction pathways and reaction fluxes shows that reactions (2) and (3) are also involved in the recombination of chain carriers. Similar schemes for ICS transformation in flames have been published previously. Unfortunately, the flame region related to the reaction fluxes studied is not always specified in the literature, e.g. Ref. [4]. In a paper [11], the reaction fluxes are given for the post-flame zone, in which the catalytic recombination has little effect on the inhibition effectiveness.

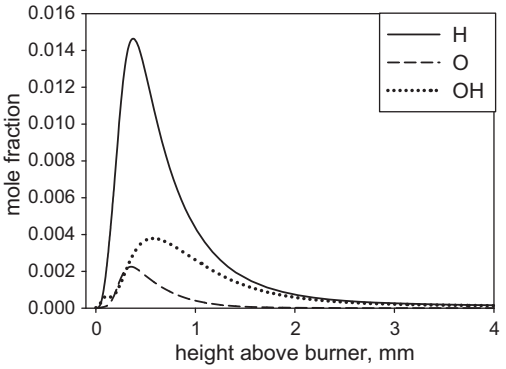

Fig. 7. Simulated spatial variations of H, O, and OH concentration in $H_2/O_2/N_2$ flame doped with 100 ppm $Fe(CO)_5$ stabilized on a flat burner at 1 bar.

4. Summary

The effectiveness of inhibition of H_2/air flames by atomic iron, expressed as the relative decrease in the flame speed with inhibitor addition, depends strongly on the equivalence ratio of the unburned gases. Both the experiment and modeling confirmed that the minimum effectiveness is observed at $\phi \approx 2$ and the maximum effectiveness is observed in the lean flames.

We were the first to measure concentrations of iron-containing products of $Fe(CO)_5$ combustion: FeO_2, FeOH, and $Fe(OH)_2$ in a $H_2/O_2/N_2$ flame at atmospheric pressure using the MBMS method.

The results obtained demonstrated that the kinetic model used in the study satisfactorily predicts the concentration profiles of the $Fe(CO)_5$ combustion products FeO_2 and $Fe(OH)_2$ in premixed $H_2/O_2/N_2$ flames of atmospheric pressure. FeOH and $Fe(OH)_2$ were shown to be the main iron-containing products of $Fe(CO)_5$ oxidation in the flame studied. In the flame reaction zone, atomic iron was shown to be the main iron-containing compound produced by the reduction of iron oxides via interaction with H, O, and H_2.

The previously proposed kinetic model for flame inhibition by iron pentacarbonyl [4] was validated by comparing the speed and structure of $Fe(CO)_5$-doped hydrogen flames. The results show that the mechanism satisfactorily predicts speeds of atmospheric-pressure H_2/air flames over a wide range of equivalence ratios and concentration profiles FeO_2 and $Fe(OH)_2$ in near-stoichiometric $H_2/O_2/N_2$ flames at atmospheric pressure.

Acknowledgement

We thank Dr. G.T. Linteris for providing the kinetic model for flame inhibition by iron pentacarbonyl.

References

[1] U. Bonne, W. Jost, H.G. Wagner, *Fire Res. Abstr. Rev.* 4 (1962) 6–18.
[2] G. Lask, H.G. Wagner, *Proc. Combust. Inst.* 8 (1962) 432–439.
[3] D. Reinelt, G.T. Linteris, *Proc. Combust. Inst.* 26 (1996) 1421–1428.
[4] M.D. Rumminger, D. Reinelt, V. Babushok, G.T. Linteris, *Combust. Flame* 116 (1999) 207–219.
[5] M.D. Rumminger, G.T. Linteris, *Combust. Flame* 120 (2000) 451–464.
[6] G.T. Linteris, V.R. Katta, F. Takahashi, *Combust. Flame* 138 (2004) 78–96.
[7] M.D. Rumminger, G.T. Linteris, *Combust. Flame* 123 (2000) 82–94.
[8] M.D. Rumminger, G.T. Linteris, *Combust. Flame* 128 (2002) 145–164.
[9] G.T. Linteris, V. Babushok, *Proc. Combust. Inst.* 32 (2009) 2535–2542.
[10] G.T. Linteris, M.D. Rumminger, V. Babushok, W. Tsang, *Proc. Combust. Inst.* 28 (2000) 2965–2972.
[11] I. Wlokas, S. Staude, C. Hecht, B. Atakan, C. Schulz, Measurement and simulation of Fe-atom concentration in premixed $Fe(CO)_5$-doped low-pressure H_2/O_2 flames, in: *Proceedings of the European Combustion Meeting: Vienna, Austria*, 2009.
[12] S. Staude, C. Hecht, I. Wlokas, C. Schulz, B. Atakan, *Z. Phys. Chem.* 223 (2009) 639–649.
[13] K. Tian, Z.S. Li, S. Staude, et al., *Proc. Combust. Inst* 32 (2009) 445–452.
[14] S. Staude, B. Atakan, *The Open Thermodynamics J.* 3 (2009) 42–46.
[15] K.B. Kim, K.A. Masiello, D.W. Hahn, *Combust. Flame* 154 (2008) 164–180.
[16] J. Zhang, C.M. Megaridis, *Combust. Flame* 105 (1996) 528–540.
[17] J.B. Howard, W.J. Kausch Jr., *Prog. Energy Combust. Sci.* 6 (1980) 263–276.
[18] N.D. Marsh, I. Preciado, E.G. Eddings, A.F. Sarofim, *Combust. Sci. Technol.* 179 (2007) 987–1001.
[19] K. Brezinsky, *Proc. Combust. Inst.* 26 (1996) 1805–1816.
[20] M.S. Wooldridge, *Prog. Energy Combust. Sci.* 24 (1998) 63–87.
[21] C. Janzen, P. Roth, B.J. Rellinghaus, *Nanoparticle Res.* 1 (1999) 163–167.
[22] C. Janzen, P. Roth, *Combust. Flame* 125 (2001) 1150–1161.
[23] H. Mache, A. Hebra, *Sitzungsber. Osterreich. Akad. Wiss., Abt. IIa* 150 (1941) 157.
[24] G.E. Andrews, D. Bradley, *Combust. Flame* 18 (1972) 133–153.
[25] F.N. Egolfopoulos, C.K. Law, *Proc. Combust. Inst.* 23 (1990) 333–340.
[26] O.P. Korobeinichev, S.B. Ilyin, V.V. Mokrushin, A.G. Shmakov, *Combust. Sci. Technol.* 116–117 (1996) 51–67.
[27] O.P. Korobeinichev, S.B. Ilyin, V.M. Shvartsberg, A.A. Chernov, *Combust. Flame* 118 (1999) 718–732.
[28] G.P. Smith, D.M. Golden, M. Frenklach, et al., GRI Mech 3.0. 1999, available at <http://www.me.berkeley.edu/gri_mech/>.
[29] T. Turanyi, I.G. Zsely, C. Frouzakis, KINALC: A CHEMKIN based Program for Kinetic Analysis, available at <http://www.chem.leeds.ac.uk/Combustion/Combustion.html>.
[30] R.J. Kee, J.F. Grcar, M.D. Smooke, J.A. Miller, A Program for Modeling Steady, Laminar, One-Dimensional Premixed Flames, report SAND85-8240, Sandia National Laboratories, 1985.
[31] R.J. Kee, F.M. Rupley, J.A. Miller, Chemkin II: A Fortran Chemical Kinetics Package for the Analysis of Gas-phase Chemical Kinetics, report SAND89-8009, Sandia National Laboratories, 1989.
[32] T. Turanyi, Mechmod v. 1.4: Program for the Transformation of Kinetic Mechanisms, available at <http://www.chem.leeds.ac.uk/Combustion/Combustion.html>.
[33] I.G. Zsely, I. Virag, T. Turanyi, FluxViewer: Visualisation Tool for Element Fluxes, available at <http://garfield.chem.elte.hu/Combustion/fluxviewer.htm>.